Analytical and numerical study of double-panel confined masonry walls

Choayb Belghiat, Jean-Patrick Plassiard, Ali Messabhia, Olivier Ple, Mohamed Guenfoud

Analytical and numerical study of double-panel confined masonry walls

Choayb BELGHIAT [a,c*], Jean-Patrick PLASSIARD [c], Ali MESSABHIA [a], Olivier PLÉ [c], Mohamed GUENFOUD [a,b].

[a] Applied Civil Engineering Laboratory / University Larbi Tébessi, Route de Constantine 12002-Tebessa, Algeria.
[b] University 8 May 1945 Guelma, BP 401 Guelma 24000, Algeria.
[c] University Savoie Mont Blanc / CNRS / LOCIE, Campus Scientifique Savoie Technolac - 73376 Le Bourget du Lac Cedex, Chambéry, France.

Mail addresses: choayb@centre-univ-mila.dz* or belghiat-choayb@hotmail.fr ; jean-patrick.plassiard@univ-savoie.fr ; a.messabhia@univ-tebessa.dz ; olivier.ple@univ-savoie.fr ; guenfoud.mohamed@univ-guelma.dz.

Abstract:

Masonry is a traditional construction method in Algeria. It is commonly used in the construction of walls, such as bearing walls or infill panels between columns and beams. Several factors make it difficult to take the material into account in structural analysis, especially in seismic cases. Therefore, engineers usually consider the masonry panel as a nonstructural element. However, the contribution of the masonry panel on the behavior of a building cannot be ignored, particularly, when talking about confined masonry walls. For this reason, a great deal of research has been conducted to generate a database that allows for masonry walls to be considered in the structural analysis. The present paper aims to contribute numerically and analytically to the study of the behavior of double-panel confined masonry walls. Thus, some of the most used analytical models are used to predict the strength and the stiffness of those structures. Moreover, a numerical micro model has been selected from the literature and validated using original experimental tests. Furthermore, one of the most used simplification strategies was adopted. The paper concluded with suggesting some analytical models and with proving the effectiveness of the numerical adopted model to simulate the behavior of confined masonry walls under Pushover tests and finally, the paper recommends future seismic study.

Keywords: Confined masonry; double-panel; analytical; numerical; micro-model.

- Declarations of interest: none

1. Introduction

Masonry is commonly used for the walls of buildings, such as bearing walls or infill panels between columns and beams. This composite material has its own mechanical characteristics, and it is strongly influenced by its environment and how it is constructed. Confined masonry walls (in this study referred to as CM walls) are common in Algeria, where the confining elements (tie-columns and tie-beams) are cast around the masonry panel. They are scientifically studied in several articles, [1], [2] and [3], among others. They are completely different from the RC frame with masonry infill. In terms of construction sequence, masonry panels are constructed first for CM walls, followed by the cast in-place of RC tie-columns and tie-beams. While the frame is constructed first in the case of RC frame with masonry infill, thereafter, panels are constructed within. Several factors make it difficult to take the masonry into account in structural analysis, especially in a dynamic environment (seismic behavior). Therefore, engineers usually consider the masonry panel as a nonstructural element. However, when talking about confined masonry, the frame/panel interaction cannot be ignored. Therefore, a great deal of research has been carried out to study the behavior of these structures applying different approaches and techniques [1–7].

Several models have been proposed in the analytical approach to predict the lateral capacities of CM walls as well as RC frame with masonry panels, in particular, their strength and stiffness. Those models consist of simplified methods and empirical formulae. In the case of RC frames with masonry panel, Fiorato et al. [8] have used the shear beam model analogy to predict the initial stiffness. In the same context, Polyakov [9] initially and thereafter Holmes [10] and Stafford Smith [11], have proposed a diagonal strut model. Flanagan et al.[12], Crisafulli and Carr [13] and others, [14], [15], [16] just to name a few, have developed the diagonal strut model to achieve more sophisticated results. Furthermore, Stafford Smith [11], Fiorato et al. [8] and Liauw and Kwan [17] have used the same concept (Diagonal strut model) to predict the lateral strength of the RC frames with masonry panel. Schmidt [18], Wood [19] and Mehrabi et al. [20] have developed the model taking into account more panel/frame connection mechanisms. In the case of CM walls, the most used approach to predict the lateral stiffness of CM walls considers the shear and flexural deformation of the wall under lateral loads. Flores and Alcocer [21], Tomaževič and Klemenc [22], and Bourzam et al. [23] have proposed a formula using this concept. Rai et al. [24] have introduced the effect of the intermediate column using a confinement factor. In the same context, Riahi et al. [25] have used a Backbone model to define the CM walls stiffness during the different stages of the damage process (Cracks initiation, significant cracks, failure). Regarding the lateral strength of CM walls, two approaches are commonly used based on failure mechanisms. The first one is derived from Mohr–Coulomb friction theory, Moroni et al.[26], D'Amore and Decanini [27], Marinilli and Castilla [28], San Bartolomé et al.[29], Matsumura [30] and Riahi et al. [25] have used and developed this approach introducing various factors while the second approach to evaluate the lateral strength of CM walls is based on the assumptions of elementary theory of elasticity. Among the authors who have used this approach: Tomaževič and Klemenc [22,31], Bourzam et al.[23], Lafuente et al.[32] and Rai et al.[24]. However, the analytical models are simplified methods and formulae to approximately predict the stiffness and resistance. They are limited to elastic domain and they are not able to reproduce the real response of those structures or simulate their local behavior with the various phenomena. For this purpose, many researchers have focused on the use of numerical models to study the behavior of masonry structures (In particular reinforced concrete frames with masonry infill or confined panels). Several numerical models are proposed in the literature, they are classified into two families according to Bicanic et al.[33], the macro modelling and the micro modelling models.

The macro modelling family includes all the simplified numerical models introduced into finite element codes. Thanks to their simplicity, they are mostly used in structural analysis as well as studying the effect of masonry panels on the behavior of large-scale masonry buildings. Crisafulli [34], Combescure [35] and Chrysostomou [16] are among the users and developers of this type of models. On the other hand, the micro modelling family includes all complex numerical models. They are formulated to study the detailed behavior of masonry structures. Because of their complexity and calculation costs, the micro models are limited to studying the behavior of laboratory samples or representative elementary samples. A complete discretization of all masonry components is adopted in these family models. The aforementioned models additionally take into

account various phenomena including the nonlinear responses, friction, plasticity, cracks and their opening or reclosure. Page [36] is the first user of the micro modelling model in the masonry domain. Cruz-Diaz [37], Lourenço and Ramos [38] and Oliveira and Lourenço [39] have used and developed more sophisticated constitutive laws. Thereafter, many micro modelling models have been proposed taking into consideration more complex factors and behavioral phenomena (Mehrabi et al. [20], Mehrabi and Shing [40], Al-Chaar et al. [41], Baloevic et al. [42], Rahman and Anand [43]). The main disadvantage of the micro models is their calculation costs and the requirement for powerful calculation machines. Moreover, they require a large amount of experiments to evaluate the corresponding parameters set. Therefore, Lourenço [44] has proposed a simplification technique which suggests lumping the mortar joints and brick-mortar interfaces in one interface element. Sutcliffe et al. [45], Cruz-Diaz et al. [46] and [47] are among the authors who adopted this simplification strategy. The present paper adopted the same simplification technique too.

The analytical models present the key factors to build macro modeling models as well as to take into account the wall contribution on structural analysis (large scale buildings). All analytical models mentioned previously are designed for the cases of simple panel masonry walls. However, how much those models are realistic toward the double-panel walls commonly used in Algeria. Consequently, the present paper makes a contribution to the numerical and analytical study of masonry panels confined by reinforced concrete frames. On the one hand, the commonly used analytical models were assessed on double-panel confined masonry walls, which represent the most used construction systems in Algeria. On the other hand, the paper reports a numerical study conducted in finite elements code Cast3m including: the characterization method, parameters calibration strategy, model validation steps and the numerical results. The adopted model aims to optimize precision and simplicity. It is based on the use of one single law for modeling lots of materials. This law is adaptable through physical parameters, which makes their calibrations a more practical tasks. Furthermore, the paper compares the two adopted construction systems using the validated model and finally suggests a future seismic study.

2. Experimental program

The present paper corresponds to the following of the work reported in Belghiat et al. [48], in which four CM walls (Two uniform CM walls and two toothed CM walls of 2.06×1.52m^2) were built. These walls comprise two masonry panels separated by a 50-mm air gap (double-panel walls see Fig. 1). The walls made of hollow bricks (300×200×100mm^3) and cement mortar were confined by a surrounding RC frames of the same section 0.25×0.25m^2, including four reinforced steel bars (12mm in diameter). The prototype studied is adopted to be the middle frame of a two-floor three-bay typical residential building which makes the vertical acting loads equivalent to 80 kN. For more details, see Belghiat et al. [48].

All the building materials were selected to correspond to Algerian standards. However, several series of tests (40 tests) were carried out to characterize the different used materials. A total of twelve 16×32 cm^2 concrete cylinders have been realized in accordance with EN 12390-2. Eight cylinders were used for compression tests and the rest for splitting tensile tests following EN 12390-3 and EN 12390-6 respectively. Six tensile tests were performed on six steel bars of 65 cm length (three on 12mm diameter and three on 6mm diameter). Moreover, three compression tests for each direction of the bricks (compared to perforations) were performed. In accordance with EN 1015-11, compression tests and bending tensile tests (three point flexural tests) were performed on 4×4×16 cm^3 mortar prisms. Table (1) below summarizes the obtained results including the results of diagonal and vertical compression tests on masonry panels.

Table 1. *Average materials parameters.*

Concrete	Test	Compression tests			Splitting tensile strength tests		
	Parameter	R_C (MPa)	E (MPa)	ε_{Peak}	R_T (MPa)		
	Uniform samples	27.93	14 333	2.82E-3	2.933		
	Toothed samples	27.66	14 740	2.75E-3	2.842		
Mortar	Parameter	Bending tensile strength (MPa)			Compression strength (MPa)		
	Uniform panels	4.72	3.80	3.89	16.73	16.25	16.26

	Toothed panels	3.86	3.70	4.21	15.13	15.50	14.00	
Brick	Load orientation compared to perforations			Perpendicular		Parallel		Vertical
	Compression strength (MPa)			0.44		5.45		0.82
Steel	Bar types			Ultimate strength (MPa)			Elastic limit (MPa)	
	Φ6			487.7			288.9	
	Φ12			601.0			482.5	
Masonry	Compression strength		Shear strength (tensile)		Young modulus		Shear modulus	
	1.13 (MPa)		0.82 (MPa)		3 919 (MPa)		1 646.5 (MPa)	

3. Analytic prediction of stiffness and first crack loading

All past analytical models were designed and assessed for the case of simple CM walls and RC frame with one masonry infill panel. In order to assess their efficiencies against double-panel walls, some existing analytical models are used in the present section to firstly deduce the lateral stiffness of the samples tested in Belghiat et al. [48]. Secondly, they were used to evaluate their lateral strengths at the appearance of first panel diagonal crack. In addition to the results in Table (1), some significant experimental results have been summarized in Table 2 from the experimental work of Belghiat et al. [48]. During these experiments, the lateral strength was not reached for none of the four walls tested. But the damage caused, suggested that the maximal experimental load applied was close to the peak of strength. Consequently, it was assumed in the following, that those maximal experimental loads could approximate the lateral strengths.

Table 2. *Estimation of significant experimental results.*

Tests	K_{Exp} (kN)	Vcr_{Exp} (kN)	Vp (kN)
PC1	176	144	247
PC2	200	195	269
PH1	201	177	263
PH2	198	177	266

Where, K_{Exp} and Vcr_{Exp} denote respectively, the initial rigidity and the first crack strength that are derived from the experimental curves of the work of Belghiat et al. [46]. Vp corresponds to the peak of strength, and is based on the assumption outlined above.

3.1. Lateral stiffness

To predict lateral stiffness of confined masonry walls, Flores and Alcocer [21] proposed a model based on the flexural and the shear deformations of the sample. Rai et al. [49] derived the stiffness taking into account the effect of the intermediate column through a confinement factor ($L_{i,s}$/P) (see Table 3). Furthermore, a Backbone model was used by Riahi et al. [50] to compute the lateral stiffness of CM walls. Figure (1) clarifies

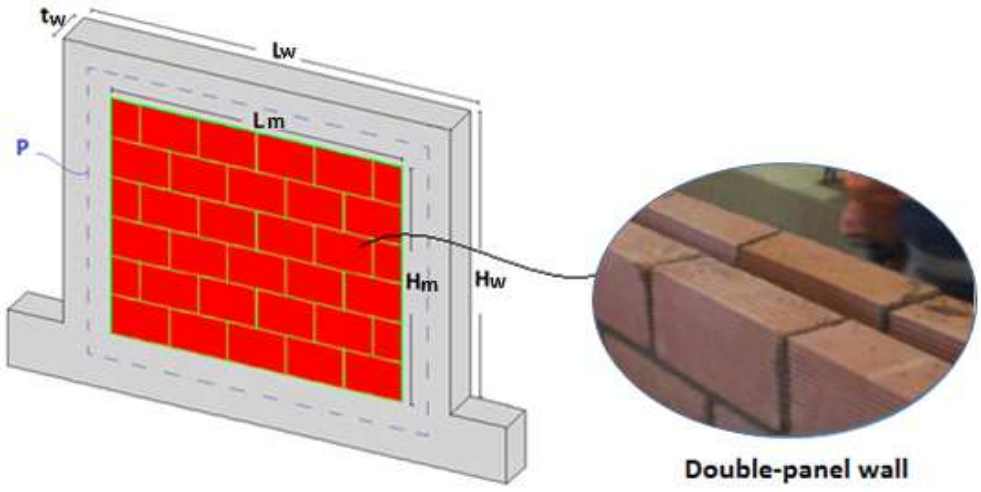

some geometrical parameters.

Fig. 1: Representation of some geometrical parameters mentioned in Table 3.

These three models are evaluated to predict the stiffness of four CM walls with uniform and toothed confinements tested previously in the work of Belghiat et al.[48]. Table (3) summarizes all the used formulae.

Table 3. *Analytical models for stiffness prediction at first diagonal crack in CM walls.*

Authors	Formula	Comments
Riahi et al. [50]	$K_{cr} = A_w \frac{\sqrt{f_m}}{\gamma_c}$	(I_m) : inertia moments of column (H_m): the height of masonry panel. (A_m) : cross section of masonry panel. (E_m, G_m) : Young and shear masonry modulus (f_m) : compressive strength of masonry. (l_{is}/P) : confinement factor defined as the ratio of the total centerline length of internal grid elements, (l_{is}), to the centerline length of confining elements at the perimeter of the wall, (P).' (A_w, H_w) : cross section and height of wall. (γ_c) : effect of unit material on the panel rigidity, equal to (1,13) for clay brick and (0,72) for concrete block.
Rai et al. [49]	$K_{cr} = K_{nc}\left(0.29 + 0.26\left(\frac{L_{is}}{P}\right)\right)$ $K_{nc} = \left(\left(\frac{{H_w}^3}{3E_m I_m}\right) + \frac{H_w}{A_w G_m}\right)^{-1}$	
Flores and Alcocer [21]	$K_{cr} = \left(\left(\frac{{H_m}^3}{3E_m I_m}\right) + \frac{H_m}{A_m G_m}\right)^{-1}$	

In figure (2), the histogram shows the ratios of obtained results to the experiments ones for each formula corresponding to all the tested samples, in which, notations PC1 and PC2 represent two samples with uniform confining elements and PH1 and PH2 represent two samples with toothed confining elements. On the one hand, the histogram shows that both models of Rai et al. [49] and of Riahi et al. [50] respectively underestimated and overestimated significantly the stiffness of all specimens. On the other hand, the model of Flores and Alcocer [21] satisfactorily predicted the initial rigidity of the walls, in which the ratio values obtained

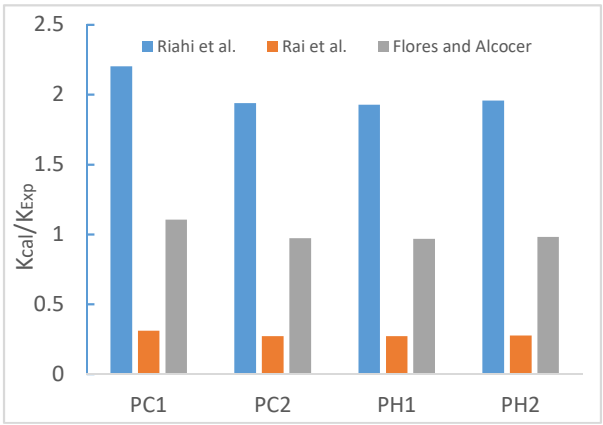

stand within interval ($0.96 \leq K_{cal} / K_{exp} \leq 1.10$) for all cases.

Fig. 2: Ratios obtained from analytical prediction of our four CM walls stiffness at first diagonal crack.

3.2. Lateral strengths

Based on the friction theory, several researchers proposed analytical models to predict the peak strength as well as the first crack strength of CM walls. The formulae proposed by Flores and Alcocer [21], Moroni et al. [26] and the Official Standard of Chile [51] represent a simple manipulation of Mohr-Coulomb theory. Matsumura [52] and Riahi et al. [50] introduced the contribution of the columns through the ratio of reinforcement bars ignoring the number of columns. Marques and Lourenço [53], along with Castilla and

Marinilli [54] used advanced statistical and regression analyses to predict the peak strength of CM walls. Rai et al. [24] introduced the contribution of tie-columns using the total longitudinal reinforcement ratio. The formulae used in this work and reported from the works [48,50,55] are shown in Table (4).

Table 4. *Analytical models for crack and peak strengths prediction of CM walls.*

	Authors	Formula	Comments
First crack strength	A. Matsumura [52]	$V_{cr} = \left(\frac{K_u}{\frac{H_w}{d}+2}\sqrt{f_m} + 0.3v_0\right) \times t_w \times j$ $j = 0.875\left(L_w - {}^{W_{tc}}/_{2}\right)$	(K_u) : reduction factor 0.64 for partially grouted walls. (d) : is the effective width of wall. (H_w, L_w, t_w, A_w): represent length, width, thickness and cross section of wall respectively. (W_{tc}) : width of tension column. (f_m, v_m, A_m) : compressive, shear strength and cross section of masonry. (v_0) : vertical applied stress. (ρ_{lc}) : ratio of longitudinal reinforcement in column. (f_y, f_c^c) : steel and concrete compressive strengths. $(L_{it}/P\ )$: defined in table (1). (N_{tc}) : number of tie-columns. (A_{tc}) : reinforcement section tie-columns.
	Chilean Standard [51]	$V_{cr} = Min(0.23v_m + 0.12v_0\ ; 0.35v_m) \times A_w$	
	Moroni et al. [26]	$V_{cr} = (0.19v_m + 0.12v_0) \times A_w$	
	Riahi et al. [50]	$V_{cr} = (0.424v_m + 0.374v_0) \times A_w \ \leq \ v_m \times A_w$	
	Flores and Alcocer [21]	$V_{cr} = (0.5v_m + 0.3v_0) \times A_w \ \leq \ 1.5v_m \times A_w$	
Peak strength	Marques and Lourenço [53]	$V_p = \left[1.0072 + 0.4897v_m + 0.5341v_0 - 0.137\left({}^{H_w}/_{L_w}\right) - 0.9966\left({}^{A_w}/_{A_m}\right)\right] A_w$	
	Riahi et al. [25]	$V_p = \left(0.21v_m + 0.363v_0 + 0.0141\sqrt{\rho_{lc} f_y f_c^c}\right) \times A_w$	
	Rai et al. [24]	$V_p = R_{nc}[2.15 + 0.7(L_{it}/P\ )]$ $R_{nc} = \min\{A_w(0.2 + 0.4v_0); 0.25\sqrt{f_m}\}$	
	Castilla and Marinilli [54]	$V_p = (0.47v_m + 0.29v_0) \times (A_w - N_{tc}A_{tc}) + 4200N_{tc}$	

The formulae mentioned in the table above were used to predict the load corresponding to the first crack of the panel and the peak strength. The obtained results are represented in a histogram in which the value deduced from each formula is expressed as a ratio with respect to the experimental results as shown in figure (3).

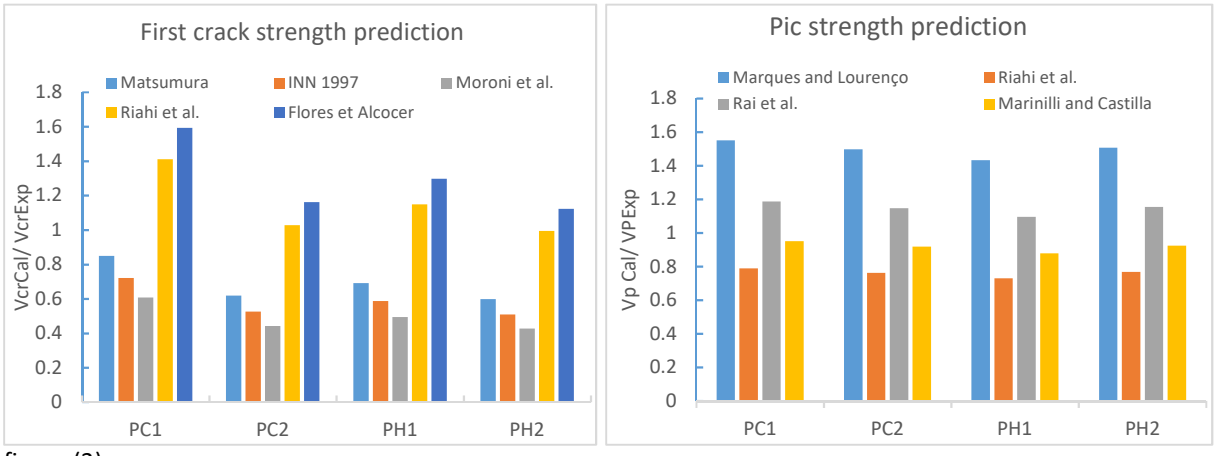

Fig. 3: *Ratios obtained from analytical prediction of our four CM walls strengths at the peak and at the first diagonal crack.*

The histograms of figure (3) indicate that the models proposed by Matsumura, Standard Chilean and Moroni et al. [26,51,52] underestimated the first crack strength and the obtained ratios are significantly low (V_{cal} / V_{exp} ≤ 0.82). It is worth noting that these models have shown good results in the work of Riahi et al. [50]. Regarding the model proposed by Flores and Alcocer [21], similar results were found in the work of [56]. The model overestimated the first crack strength (1.12 ≤ V_{cal} / V_{exp} ≤ 1.6) but still stands as a good approximation indicator. The best results have been obtained using the model of Riahi et al [50], in which the various ratios achieved still stand in the interval [0.99; 1.41]. Regarding the peak strength prediction, the model of Marques and Lourenço [53] overestimated the peak strength (1.43 ≤ V_{cal} / V_{exp} ≤ 1.55). The model of Rai et al. [24] overestimated this strength but still stands as a good indicator in which the ratio values obtained stand within interval [1.1 ; 1.9]. Moreover, the model of Riahi et al. [25] underestimated the peak strength in all cases (for all samples), similar results were found in [55]. The best prediction, in a conservative way, is given by the model of Castilla and Marinilli [54] (0.88 ≤ V_{cal} / V_{exp} ≤ 0.95).

4. Numerical approach and calibration

Away from the analytical models, several numerical models have been proposed in the literature to study the behavior of CM walls thoroughly. According to Bicanic et al. [33], these models can be classified in two approaches: macro-modeling approach and micro-modeling approach. The model adopted in this paper carries out an optimum choice between the two approaches. It belongs on the one hand to the micro modeling approach, which reproduces the detailed behavior. On the other hand, it adopts one of the simplification techniques of the macro modeling approach. This simplification simulates the mortar joint and the two interfaces as a single homogeneous element, as proposed by Lourenço [44].

4.1. Adopted model

Here, a mixed approach was applied between the macro modelling and the detailed micro modelling. The joint of mortar and its interfaces with bricks are considered as one homogeneous material. Generally represented with interface element, an approach with volumetric finite elements were chosen in the current work. Apart from respecting the geometry more precisely, this choice was motivated by the fact that all of the brick, the concrete and the mortar materials exhibit a quasi-brittle behavior. These allows the use of the same constitutive law for all materials involved, by this way avoiding the limitation of the constitutive law available in the used software.

The model adopted in this work is introduced into finite elements code Cast3m with a numerical explicit approach. Concrete and bricks are modelled by eight nodes cubic elements with the adapted law proposed, developed and implemented by Sellier et al. [57]. While the steel bars are represented by two nodes segments with elasto-plastic perfect law. Regarding the mortar joints, the Lourenço [44] simplification is adopted. Consequently, hexahedral elements are used with Sellier et al. [57] law, but first, calibrated in order to simulate the combined behavior of the mortar and the two surrounding contact interfaces. Sellier et al. [57] law is implemented in finite elements code Cast3m under instruction “ENDO3D”. This constitutive law involves both elastoplasticity and damage in tension and compression states. It is initially proposed for concrete combining an orthotropic Rankine criterion in traction and the Drucker-Prager criterion in compression. The Rankine criterion (f_i^t) is defined in the principal base of undamaged stresses tensor (σ_i) as a function of the effective tensile strength in a principal direction of stress (R_i^t) and its expressed as follows [58]:

$$f_i^t = \sigma_i - R_i^t$$

The Drucker Prager criterion used in compression and for modeling the plastic strain due to the propagation of micro cracks induced by shear stresses, is described as follows:

$$f^c = \left(\sqrt{\frac{\sigma_{ij}^d : \sigma_{ij}^d}{2}} + \delta \frac{Tr(\sigma_{ii})}{3} \right) - R_c \left(\frac{1}{\sqrt{3}} - \frac{\delta}{3} \right)$$

Where (R_c) is the compressive strength, (δ) the Drucker Prager confinement coefficient, (σ_{ij}^d) the diviatoric components of stress tensor [58]. Figure (4) shows a multidimensional plot of the interaction of Drucker Prager and Rankine criteria.

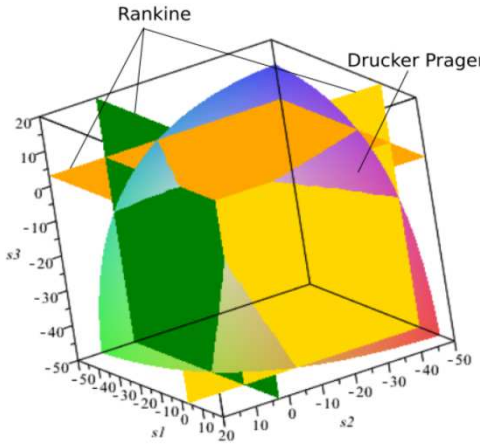

Fig. 4: *Drucker Prager and Rankine criteria interaction*[58] .

Moreover, Sellier's et al. [56] law is formulated to describe, in an anisotropic way, the cracking mechanism. The damaging effects are also considered for tensile, compression and shear states. Furthermore, the constitutive law takes into account hysteresis effects, plasticity and cracks reclosure. The final form of the constitutive equation behavior of the Sellier's law is expressed as follows :

$$\sigma_{ij} = (1 - D^c).(1 - D^t).S^0.\varepsilon_{ij} + (1 - D^c).D^t.S^0.\left(\varepsilon_{ij} - \varepsilon_{ij}^f\right)$$

In which, (D^t) is defined as tensile damage tensor, (D^c) the compression damage tensor corresponding physically to the crashing of materiel. (S^0) is the stiffness matrix of undamaged material and (ε_{ij}^f) is the inelastic strain associated with the crack opening. Those internals variables were evaluated based on thermodynamics framework using the free energy potential. More details can be found in [57]. Other aspects are also combined to the mechanical behavior, such as chemo-mechanics, poro-mechanics, but they were not required in the present study. It is consequently appropriate to simulate the directional properties of fragile materials [57]. The following figure (5) illustrates the response under cyclic uniaxial-tension-compression test reported in [57].

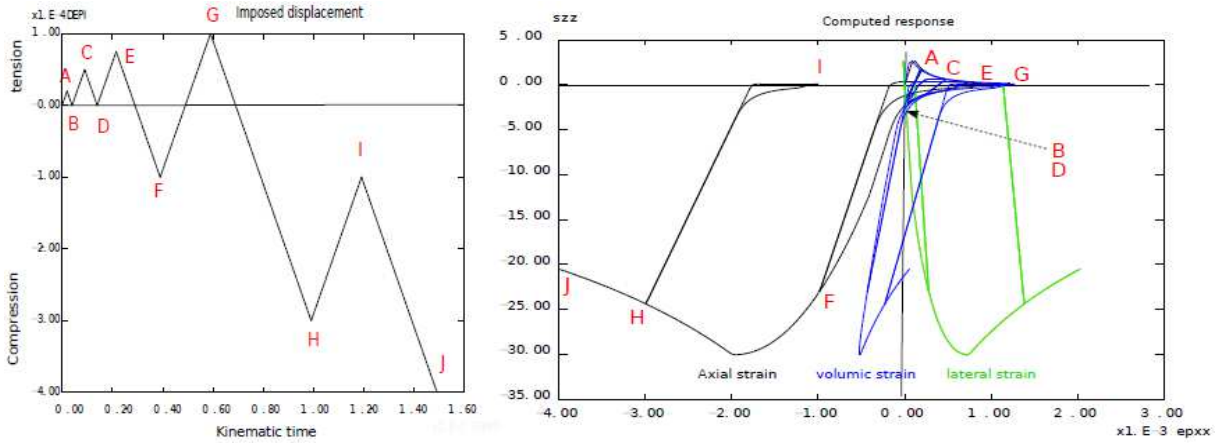

Fig. 5: *Behavior law obtained from cyclic uniaxial-tension-compression test* [57] .

The main advantage of the adopted model is its ability to simulate all materials by calibrating their intrinsic parameters. These physical and mechanical parameters can be identified through a simple and commonly characterization tests. Using the same law for all materials provides some interest regarding the convergence of numerical calculations. Regarding the modeling technics presented in previous studies (2D modeling approach like in [59]), the three dimensional discretization was adopted to match the all dimensional characteristics [60]. The modelling considers the mortar joints and the bricks geometries, unlike the commonly

used technics which consider zero thickness interface elements. Adopting the Lourenço simplification technique, mortar joint and interfaces are considered as continuum elements [44].

4.2. Parameters calibration method

According to Domede et al. [61], two steps are required to use Sellier's et al. [57] law in the case of masonry structures. The first is pure experimental characterization of the masonry components while the second step consists of numerical simulations to produce the homogenous parameters. The used calibration method in this paper is inspired by the methodology proposed by Domede et al. [61]. Therefore, three sample classes were used in the experimental research presented in this work: material samples, partial structure samples and CM wall samples. The material samples are used to define the majority of individual parameters of steel, mortar, brick and concrete. During the characterization tests, the potential risk of damages of materials imposed to remove the camera during the tests. Consequently, the lack of measuring instruments caused some limitations as regards determining the parameters. Then the numerical simulations of these tests addressed these limitations by determining the missing parameters. The obtained results from the first samples' group formed a base for the second samples' group (passage from the material scale towards the local scale).

The first test of the second group is a three points bending flexural test on the composed interface sample. The test aims to deduce the tensile strength, the Young's modulus and the tensile fracture energy of the mortar/brick interface and that of the concrete/brick interface too. On the one hand, the tensile strength is deduced experimentally and the tensile fracture energy by an analytical formula from [62]. On the other hand, the Young's modulus is numerically recalibrated to obtain a good coincidence of curves. In the case of mortar, concrete and brick, the used parameters are reported from the first samples group results (material scale). Afterwards, the obtained parameters from the interface bending test are injected into the triplet model test. The interface Drucker-Prager (referred in this paper by D-P) confinement factor is calculated analytically as reported in [61] and its compressive strength is numerically recalibrated until the coincidence of the numerical and experimental curves. Next, the interface parameters previously obtained are injected into the model of vertical compression panel test. The brick Young's modulus is deduced thanks to the image correlation technique [63] and its compressive strength from the compression test on the brick unit of the first samples group. The tensile fracture energy and the strength of the brick are analytically calculated as reported in [62]. Finally, the D-P confinement factor is numerically recalibrated until the coincidence of curves. The last test in partial structures group is a diagonal compression test on a masonry panel. The parameters set used in the previous vertical compression test are adopted. Due to the anisotropic nature of the masonry, a significant dissimilarity between the numerical curves and the experimental one is obtained. Thus, the Young's modulus, the compressive strength and the tensile strength of bricks required a readjustment to this new test configuration. The experimental stiffness and the initial slope of the strain-strain curve obtained, according to the standard [64], are used to determine the shear coefficient and the diagonal Young's modulus of the brick. Thus, the tensile strength and the diagonal compression strength of the bricks are adjusted to match the coincidence of curves.

The last group (CM wall samples) represents two types of tests (monotonic and cyclic loading). In the first testing type, the diagonal compression test parameters are used for the bricks and the interfaces, whereas the concrete and steel are simulated according to the first samples group (Materials). Subsequently, the same set of parameters is introduced in the first model of cyclic tests to calibrate the Drucker-Prager plastic deformation characteristic associated with the damage (EKDC), which manages the reversibility of the response. Finally, the second model of cyclic tests validated this final parameter set.

4.3. Numerical results

The present section reports the characterization processes and the validation of the adopted model by the partial structures as well as the CM walls samples. The section also shows the competency of the model to simulate the CM walls behaviors under Pushover tests using the calibrated parameters with characterization

tests. It is worth noting that a software dedicated to digital image correlation technique was used on most tests reported in Belghiat et al. [48]. This software is named 7D and works by comparing images provided from a tested sample at different experimental stages, details of computing strategy are reported in [65].

4.3.1. Interfaces

In order to calibrate the interface parameters and to demonstrate the effectiveness of the adopted model to simulate the behavior of these elements, two test types were carried out: Three point bending flexural tests on composed interface samples and shear tests on confined masonry triplets (see Fig.6).

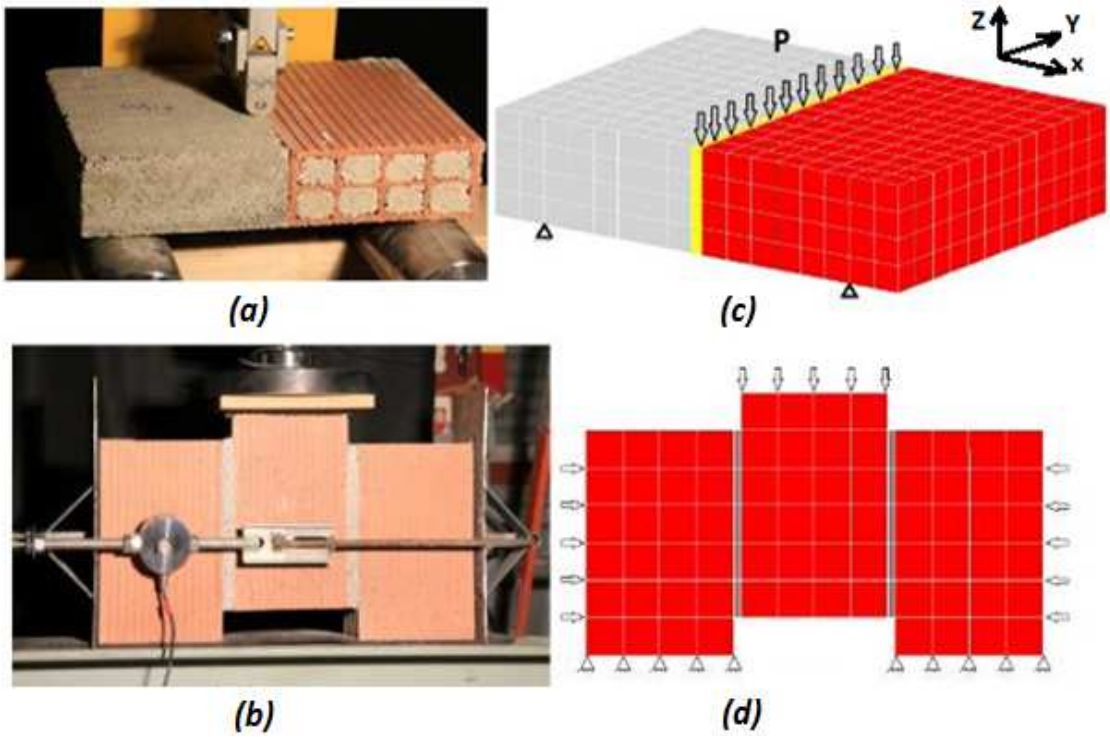

Fig. 6: *Physical and numerical interfaces models: (a) Experimental composed interface model, (b) Experimental triplet model, (c) numerical composed interface model, (d) numerical triplet model.*

The interface fracture energy, tensile strength and Young's modulus are calibrated using three point bending flexural tests. Initially, the tensile strength is deduced experimentally taking into account the shrinkage effect of the mortar and posing process of the units as reported in the work of Lourenço [44]. Consequently, the net contact area of the interface is restricted to 59% of the total area. The tensile fracture energy is deduced using the formula (1) proposed by Drougkas [62]. Young modulus is then calibrated to reproduce the experimental curve.

$$G_f^I = 0.025(2f_t)^{0.7} \quad (1)$$

Afterward, those traction interface parameters are used into shear confined triplet tests. While, the D-P confinement factor is calculated analytically via the internal friction angle using the formula (2) reported from the work of Domede et al. [61], the compressive interface strength is calibrated until the curves coincidence. The adopted parameters for the interface are summarized in table (5) , where, (R_t), (G_f^t), (E), (δ) and (R_c) represent respectively: tensile strength, tensile fracture energy, Young's modulus, D-P confinement factor and the compression strength of the interface.

$$\delta=\frac{2\sqrt{3}\times\sin\emptyset}{3-\sin\emptyset} \quad (2)$$

Table 5. *Parameters set for interface element (Triplet and composed samples).*

Parameter	Mortar/brick Interfaces		Concrete/brick Interfaces		
	Ep1	Ep2	Ep1	Ep2	Ep3
R_t (MPa)	0.06	0.12	0.25	0.105	0.18
G_f^t (MJ/m^2)	1.5e-3	1.8e-2	5.1e-2	1.1e-2	9.1e-2
E (MPa)	350	550	800	1000	180
δ	1.34	1.34	1.34	1.34	1.34
R_c (MPa)	9.24	9.24	9.25	9.25	9.25

During the numerical simulations the applied boundary conditions are represented in images (c) and (d) of figure (5). The vertical loads are applied with displacement controlled condition and the lateral load with load controlled condition (to apply the confinement force on masonry triplets). As shows figure (7), on the one hand, the obtained results from the three points bending flexural tests as well as the experimental ones, are represented as curves translating the deflection of composed samples as function of the applied loads (For three concrete/brick interfaces and two mortar/brick interfaces). On the other hand, the shear tests results applying four confinement values are translated into Mohr-Coulomb failure criterion. As shown in figure (7), the experimental and the numerical criteria are classified in two types, initial and residual criteria. The initial criterion relates the ultimate strengths of the interfaces with the applied confinements, while, the residual criterion represents the residual strengths of the interface as a function of the applied confinements.

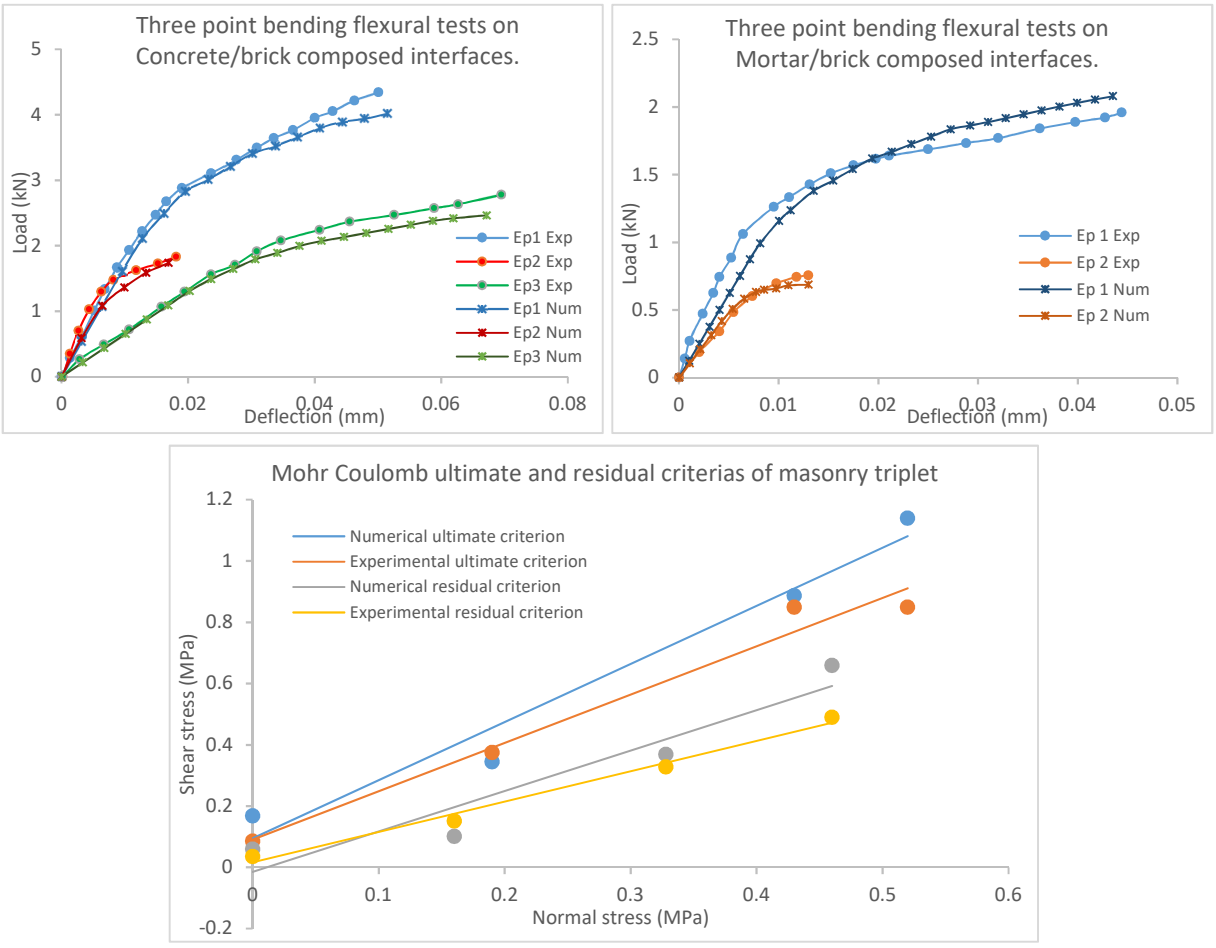

Fig. 7: *Experimental Vs numerical curves from tests on interface elements.*

As shown in figure (7), the adopted model reproduces accurately the response of composed concrete/brick and mortar/brick interface samples under three points flexural test. Thanks to the displacement directions map provided by the software 7D [65], the correlation images technique showed that the lower interface area is a tension zone and that the upper area is a compression zone (Fig. 8-a). The same

phenomenon has occurred in the numerical model (qualitative comparison) as reflected by the distribution of volumetric deformations illustrated in figure (8-b). Otherwise, the adopted model also suitably simulates the ultimate and residual criteria, more precisely, in the confinement range of 0 to 0.2 MPa. It could then reproduce the response of confined triplets under shear tests. Similar failure modes were witnessed in all tested triplets, the middle brick slips downwards with interfaces detachment. The numerical model has succeeded in reproducing this failure mode as demonstrated in the images (c) and (d) of figure (8).

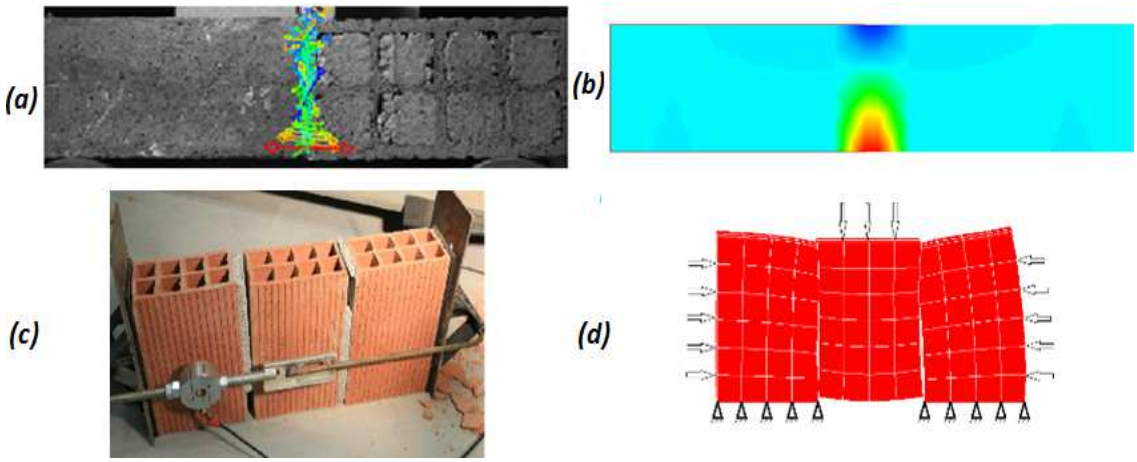

Fig. 8: Experimental and numerical tests result: (a) displacement directions of bending interface, (b) volumetric deformations of the interface, (c) experimental triplet failure mode, (d) numerical triplet failure mode.

4.3.2. Masonry panel

The second step aims to simulate, using the same model, the masonry panel behaviors under the

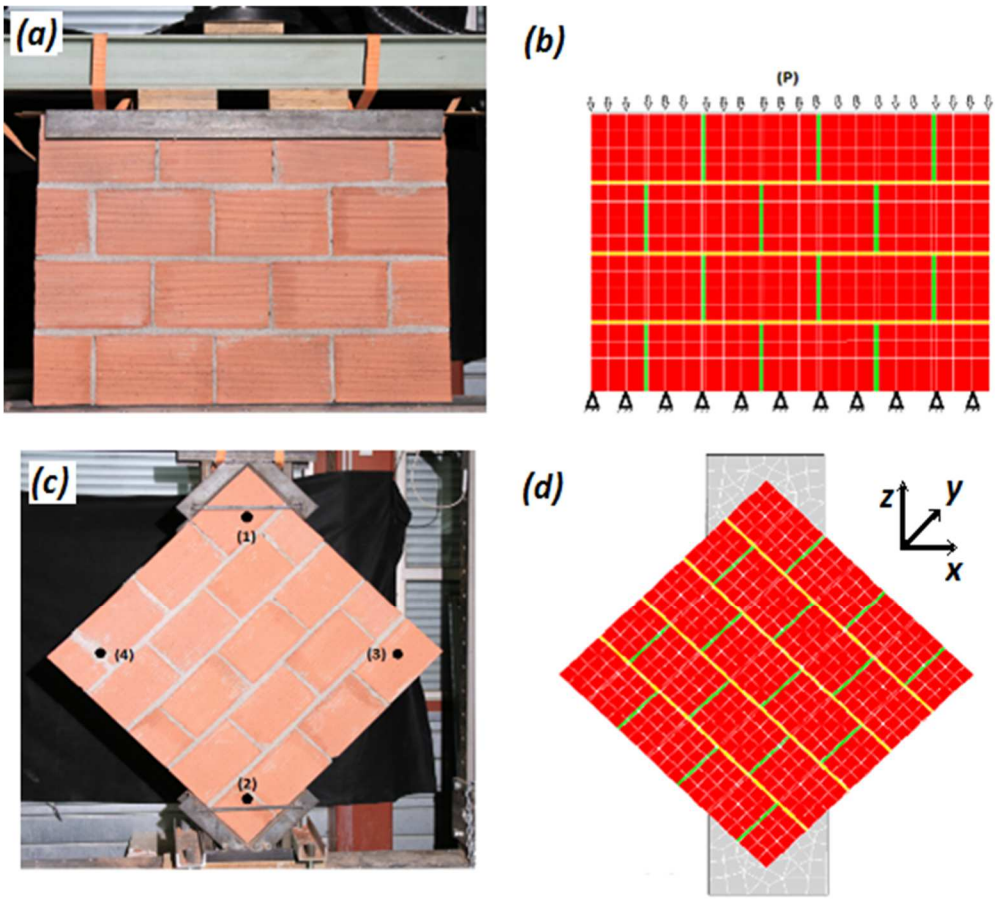

diagonal and vertical compression tests (see Fig 9).

Fig. 9: Vertical and diagonal compression tests on masonry panels: (a, c) Physical models, (b, d) numerical models.

The interfaces parameters are reported from table (5), and the bricks parameters from material characterization tests as represented in table (6), while the Drucker-Prager confinement coefficient of bricks is recalibrated until the coincidence of the curves. Young's modulus is determined experimentally from the initial slope of the compression test curve. However, the fracture energy is analytically calculated using the formula (1) as reported in Drougkas et al. [62] and the tensile strength is estimated to be 9% of the compressive strength as proposed in Drougkas et al. [62].

Table 6. *Parameters set of masonry panels (Vertical and diagonal compression tests).*

Parameters	Brick	Interfaces
R_c : Compression strength (MPa)	0.85	9.24
R_T : Tensile strength (MPa)	0.1	0.12
E: Young modulus (MPa)	175	348.5
GFT: fracture tensile energy (MPa)	3.6^{E}-2	2.9^{E}-3
DELTA : Drucker-Prager confinement factor	0.78	1.34

During both tests the load was applied in (Z) direction by imposed displacement condition. In the vertical compression test, the lower panel surface was blocked in (Z) direction. Similar boundary conditions are used on contact areas (100x300 mm^2) of panel with metallic supports in diagonal compression test (Z direction were blocked). As shown in figure (10), the experimental and numerical panel responses under the vertical compression were translated as curves of variation of the displacement as function of the applied load. Similarly, the resulted curves of diagonal compression tests are illustrated in figure (10).

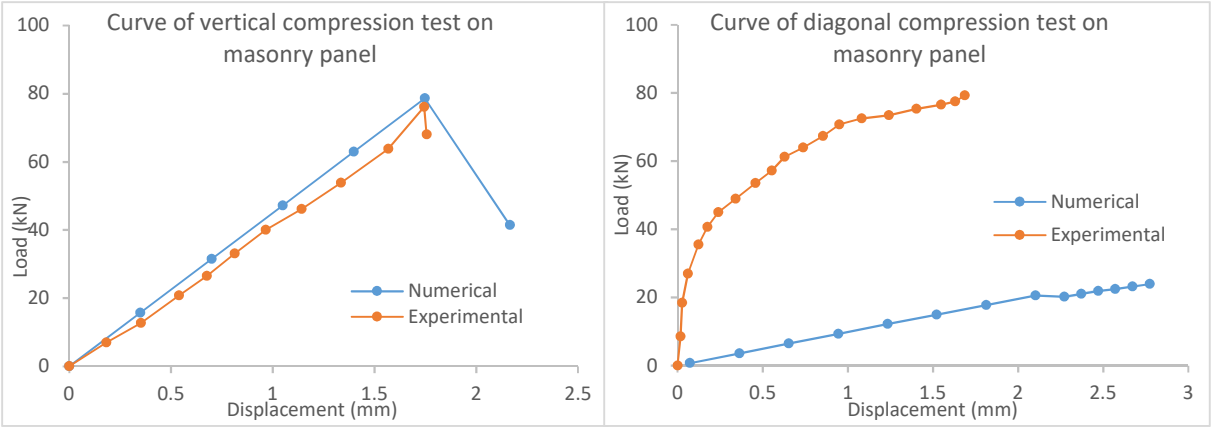

Fig. 10: Experimental and numerical load-displacement curves of vertical and diagonal compression tests.

From the curves of figure (10), the model properly simulates the initial rigidity and the maximum loading of the panel under the vertical compression test, but the failure that occurred during the experiment was more brittle than the one produced in the numerical model. The effect of representing the anisotropic hollow bricks by a continuous volume of cubic elements can justify the post peak behavior difference. Regarding the diagonal test, the numerical curve reflects a much lower stiffness than the experiment with numerical stiffness equal to 3.4% of the experimental one. The given ratio ensures that the Young modulus of the brick in the vertical direction and in the diagonal direction is not the same and that the anisotropy of brick affects strongly the directional proprieties of bricks. Also, according to Shaan and Torrenti in [66], the Young modulus of the brick can vary between 7220 MPa, in parallel to perforations to 405 MPa in perpendicular to perforations. Due to difficulties of determining the Young's moduli of brick in any case, a numerical calibration of the diagonal Young modulus has been engaged. The slopes of load-displacement curve and the stress strain curve, deduced by the instructions of the standard diagonal compression test on masonry panel [64], are used on the one hand to recalibrate the diagonal Young modulus. On the other hand, the compressive and tensile strengths are recalibrated until the total coincidence of the curves. Finally, the recalibrated parameter set used

in the numerical model is reported in table (7). The estimation of the value of the diagonal Young modulus is in good agreement with those of Shaan and Torrenti [66].

Table 7. *Recalibrated parameters set used for the bricks in diagonal compression test.*

Parameters	Brick
R_c : Compression strength (MPa)	3.25
R_T : Tensile strength (MPa)	2.75
E: Young modulus (MPa)	7212
GFT: fracture tensile energy (MPa)	3.1-4
DELTA : Drucker-Prager confinement factor	0.78

The obtained load-displacement curve after the recalibration of the bricks parameters are represented in figure (11). Moreover, thanks to the displacements of the points 1 to 4 as shown in figure (9-c) obtained by the images correlation technique, the variation curve of the shear stresses as a function of the angular deformations of the panel were outlined according to the instructions of the standard of the diagonal

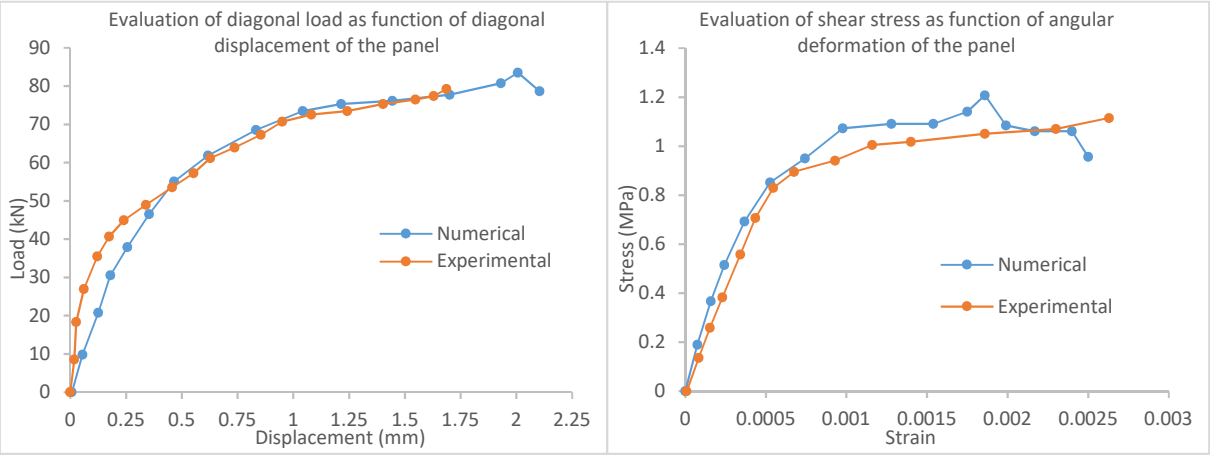

compression test on masonry panels [64] (See Fig. 11).

Fig. 11: *Experimental and numerical obtained curves of diagonal compression tests after recalibration.*

The model efficiency was proved by the reproduction of the response of the panel under the diagonal compression load in terms of the variation of the loading as a function of displacement as well as the variation of the stress as a function of strain (Fig.11). Furthermore, the concordance of the numerical model with the physical one has been validated by the uniformity of the failure modes obtained in both cases. Qualitative comparison was then illustrated by images of figure (12), in which the image (a) presents the logarithmic deformations provided by the software 7D [63] on the physical model while the image (b) presents the

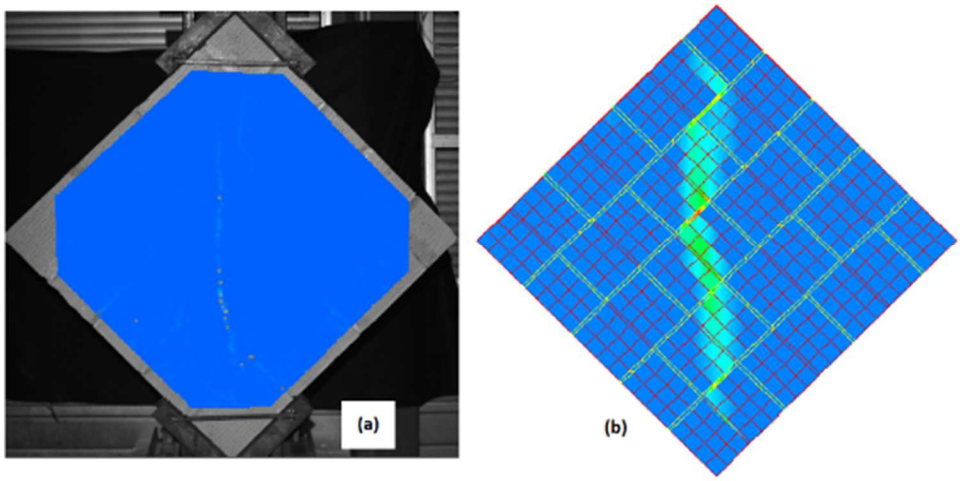

volumetric deformations thanks to the internal variables on the numerical model.

Fig. 12: *Panel failure mode under diagonal compression, (a) logarithmic deformations using the software 7D* [63]*, Volumetric deformations using the internal variables TEPS.*

5. Confined masonry walls simulations

The reported Pushover tests from Belghiat et al.[48] on confined masonry walls were used in this section to validate the adopted model. Four tests were carried out, the first one is a monotonic lateral loading test on CM wall with uniform confining elements (PC1), whereas the second one is a loading unloading test on CM wall with uniform confining elements (PC2). The third test is a monotonic loading test on a CM wall with toothed confining elements (PH1) and the last one is a loading unloading test on a CM wall with toothed confining elements (PH2). Thanks to the symmetric shape of the samples, the numerical models were limited to half of the studied walls in the out-of-plane direction. The two types of models as well as the detailed discretization are shown in figure (13). During the numerical tests, the vertical load (80 kN) was uniformly applied with load control conditions on the upper section of the beam. The lateral loading was applied with displacement controlled conditions firstly in a progressive way and secondly in a loading-unloading way to ensure the similarity of loading conditions between the numerical and experimental tests. Alternatively, the symmetric plan was blocked following the (Y) direction and the tie-beam volume following the three directions (X, Y and Z).

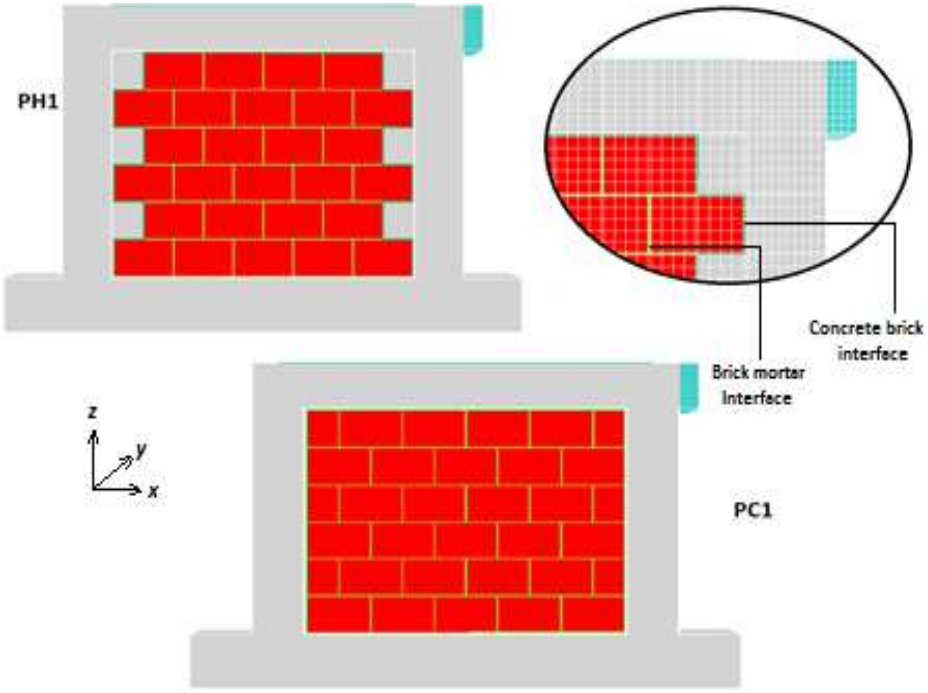

Fig. 13: *Finite element model for confined masonry walls introduced in software Cast3m.*

The parameters sets used were quoted from the previous characterization tests (Tables 5, 6 and 7). Table (8) reports more details about the adopted parameters sets for each sample's components where (R_c) and (R_t) represent respectively the compressive and the tensile strengths. The parameters (E) and (GFT) are the Young modulus and the fracture energy in tension and (EKDC) represents the plastic deformation associated to compression damage.

Table 8. *Parameters adopted set for Pushover tests on confined masonry walls.*

Samples	Parameters	Concrete	Steel ⌀ 6	Steel ⌀ 12	Brick	Horizontal Brick mortar Interface	Vertical Brick mortar Interface	Concrete brick interface
PC1	R_c (MPa)	29.89	390	506	3.25	9.24	9.24	9.25
	R_t (MPa)	2.83	390	506	2.75	0.12	0.12	0.25
	E (MPa)	14370	150558	170558	7212	348.5	348.5	500
	GFT (MPa)	8^{E}-3	/	/	3.1^{E}-4	2.9^{E}-3	2.9^{E}-3	1.5^{E}-2
	EKDC	9^{E}-4	/	/	9^{E}-5	1^{E}-4	1^{E}-4	1^{E}-4
PC2	R_c (MPa)	28.24	390	506	3.25	9.24	9.24	9.25
	R_t (MPa)	2.78	390	506	2.75	0.12	0.12	0.25
	E (MPa)	14370	150558	170558	7212	348.5	348.5	500
	GFT (MPa)	8^{E}-3	/	/	3.1^{E}-4	2.9^{E}-3	2.9^{E}-3	1.5^{E}-2
	EKDC	9^{E}-4	/	/	6.5^{E}-5	1^{E}-4	1^{E}-4	1^{E}-4
PH1	R_c (MPa)	26.26	390	506	3.25	9.24	9.24	9.25
	R_t (MPa)	2.78	390	506	2.75	0.12	0.12	0.25
	E (MPa)	14420	150558	170558	7212	348.5	348.5	500
	GFT (MPa)	9^{E}-3	/	/	3.1^{E}-4	2.9^{E}-3	2.9^{E}-3	1.5^{E}-2
	EKDC	4^{E}-4	/	/	9^{E}-5	1^{E}-4	1^{E}-4	1^{E}-4
PH2	R_c (MPa)	26.26	390	506	3.25	9.24	9.24	9.25
	R_t (MPa)	2.78	390	506	2.75	0.12	0.12	0.25
	E (MPa)	14420	150558	170558	7212	348.5	348.5	500
	GFT (MPa)	9^{E}-3	/	/	3.1^{E}-4	2.9^{E}-3	2.9^{E}-3	1.5^{E}-2
	EKDC	4^{E}-4	/	/	6.5^{E}-5	1^{E}-4	1^{E}-4	1^{E}-4

The obtained results were translated as response curves which relate the variation of lateral loading as function to the lateral displacement of the beam. Figure (14) shows the numerical curves versus the experimental ones for all samples, including the monotonic tests and the loading-unloading tests.

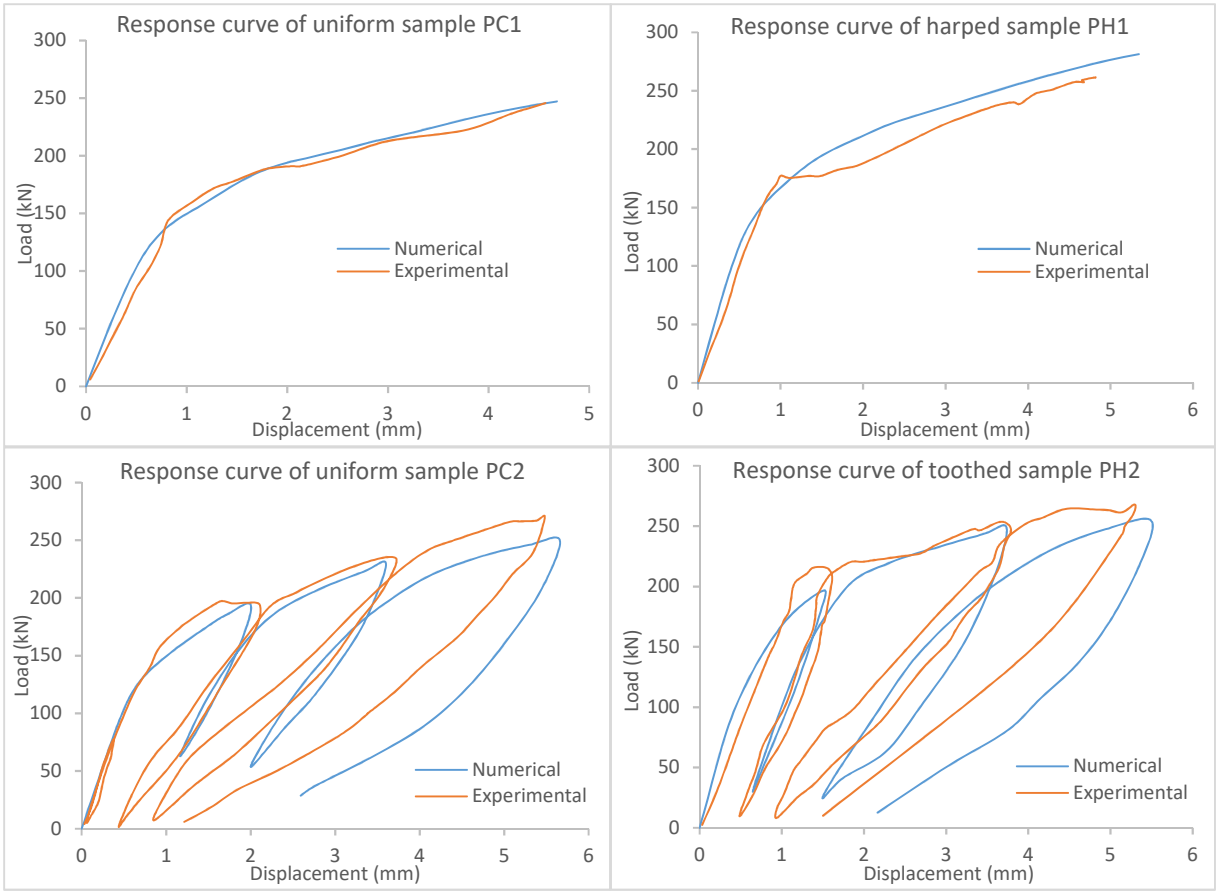

Fig. 14: *Numerical and experimental load-displacement curves of uniform and toothed samples under monotonic and loading unloading conditions.*

As shown in figure (14), the model reproduces accurately, in monotonic loading conditions, the uniform and the toothed samples responses. It simulates correctly the initial rigidity of samples PC1 and PH1 and their nonlinear responses. Moreover, the model has succeeded to simulate the initial rigidity, degraded rigidities and the unloading responses of the uniform and the toothed samples under loading unloading conditions (PC2 and PH2). Furthermore, the cracks propagation path of the numerical model and the experimental one were compared qualitatively for all samples. Figure (15) represents the experimental cracks propagation paths obtained thanks to the logarithmic deformation provided by the software 7D [63] and the numerical cracks propagation path produced by the volumetric deformations thanks to the internal variable (TEPS) of Sellier's law [57].

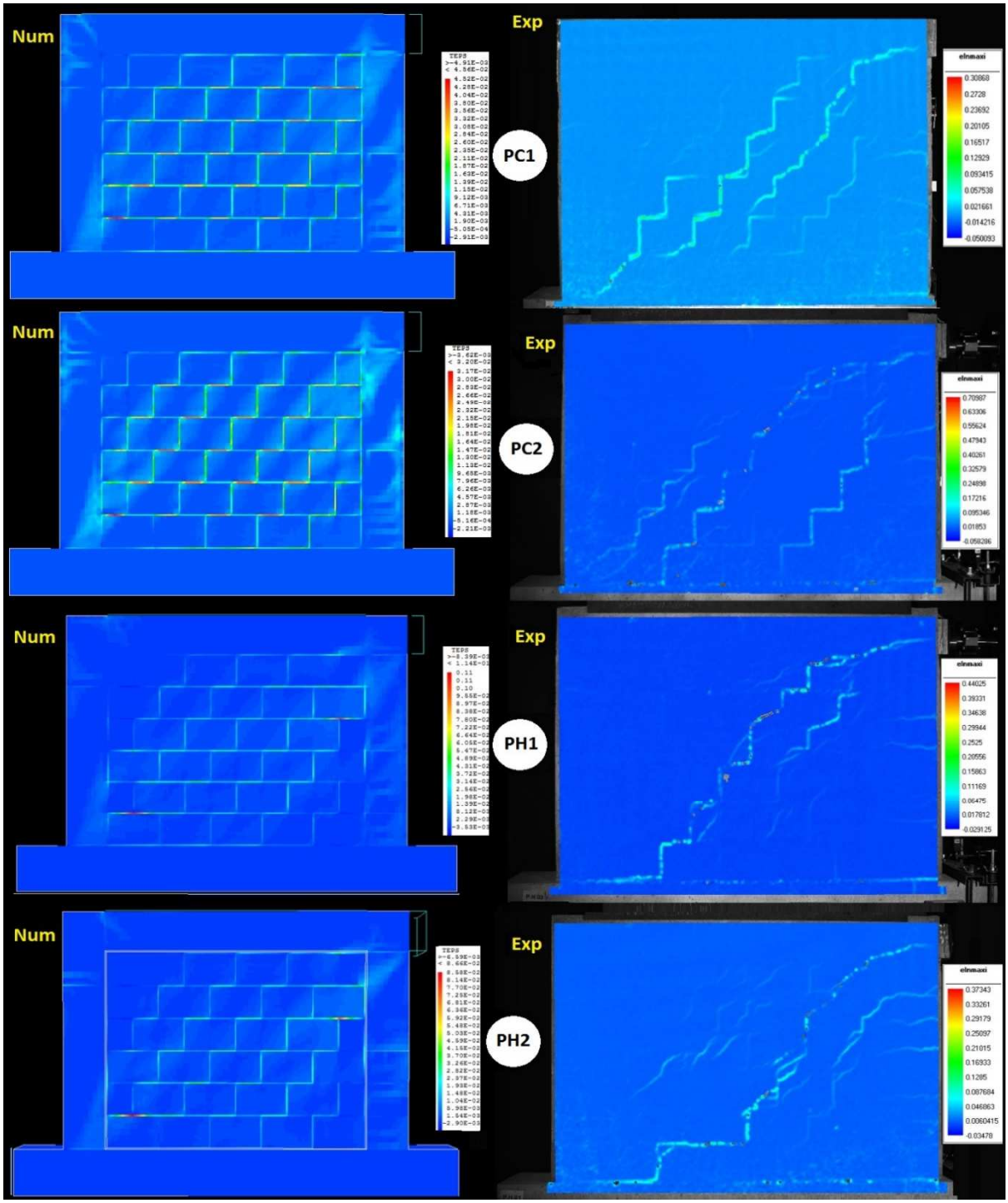

Fig. 15: *Numerical Vs experimental cracks propagation paths for all samples.*

Comparing the numerical model and the physical one from figure (15), the flexural cracks appeared, on the one hand, on the loaded column are similar in all samples in terms of orientation and propagation along the column height. On the other hand, the diagonal cracks propagated in the panel, in the numerical model, have the same orientation, shape and diffusion area of those that appeared in the physical model (experiment). Furthermore, the cracks continuation phenomena from the confinement element (column) toward the panel were also captured in the numerical model. Particularly, the cracks of the top right corner propagated through the masonry panels. Consequently, the efficiency of the model to simulate the CM walls behaviors were proved globally by load-displacement response curves and in detail using cracks propagation paths.

In order to further investigate the efficiency of the numerical model to simulate the seismic behavior of CM walls with various frame/walls connections (Uniform and toothed confinements), two parameters were studied for the numerical model and the experimental one, the rigidity degradation and the energy dissipation capacity. For this purpose, the realized loading unloading cycles were used to illustrate the evaluation of the rigidity degradation (The rigidity of each cycle as a function of the displacement associated with the loading branch and exactly the end point of the linear branch). Furthermore, those cycles were used to illustrate the evaluation of the cumulative dissipated energy for the two types of samples (the dissipated energy deduced by the area under the curve of each cycle as a function of the maximum displacement of the cycle). Figures (16) and (17) present the numerical versus the experimental obtained curves concerning the rigidity degradation and the dissipation energy capacity respectively. Otherwise, the obtained calculation results are presented in table (9).

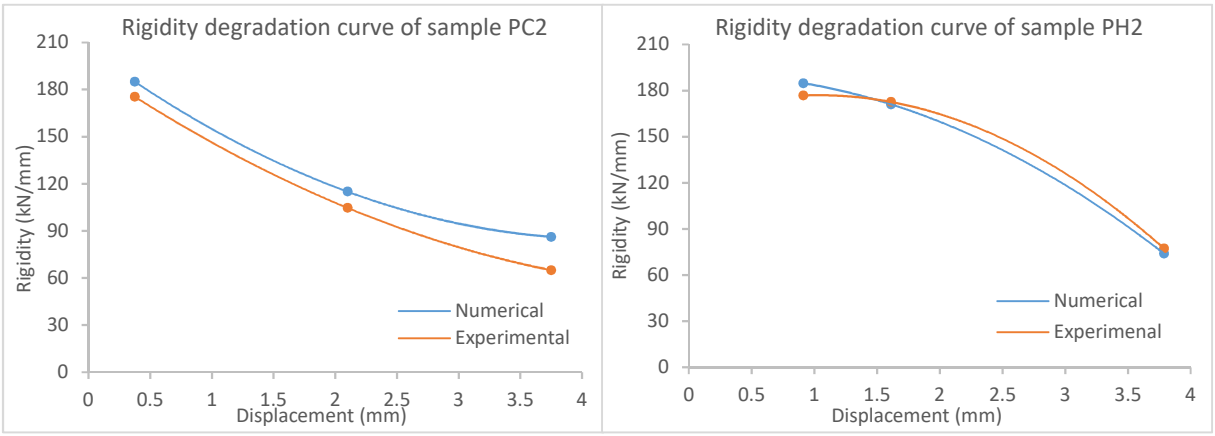

Fig. 16: Numerical versus experimental evaluation curves of rigidity as function of displacement.

Fig. 17: Numerical versus experimental evaluation curves of cumulated dissipated energy as function of maximal displacement cycle.

As show in figure (16), the model has properly simulated the rigidity degradation of the two sample types (uniform and toothed confinements). The shape of the numerical curves was similar to those of the experimental ones. The error margin, as shown in table (9), remained within the range of 5% to 32% in the uniform sample case, and 4% in the toothed sample case. Regarding the numerical and the experimental curves of figure (17), the model produced a perfectly coincidence curve to the experimental results of the uniform sample, which means that the model dissipates the same quantity of energy through the loading-unloading process compared to the experimental result. The measured error margin in the case of toothed sample remained within the range of 8% to 0% (See table 9).

Table 9. *Calculation results of rigidity degradation and dissipation energy capacity.*

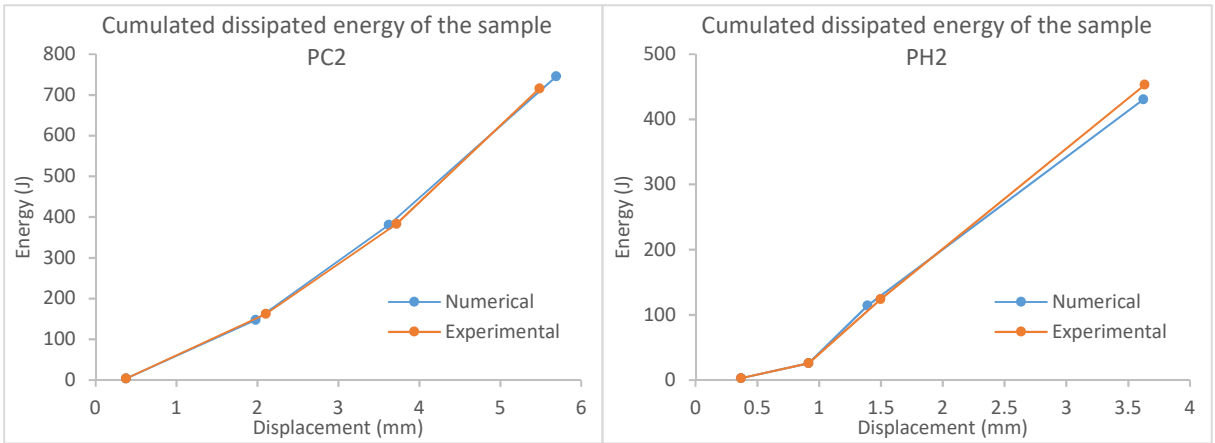

Parameter	Sample	Test	Cycle 1	Cycle 2	Cycle 3	Cycle 4

Rigidity degradation (kN/mm).	Uniform	Experimental	175,44	175,44	104,66	65
		Numerical	185	185	115	86,22
		Error (%)	5	5	10	32
	Toothed	Excremental	176,78	176,78	172,56	77,2
		Numerical	184,8	184,8	171	73,87
		Error (%)	4	4	1	4
Cumulated dissipated energy (J).	Uniform	Experimental	3,442	162,392	383,012	715,251
		Numerical	3,526	147,18	380,45	745
		Error (%)	2	9	1	4
	Toothed	Excremental	2,694	25,861	123,723	453,016
		Numerical	2,696	25,795	113,93	430,45
		Error (%)	0	0	8	5

The results above indicate the effectiveness of the used finite elements model to reproduce the characterization tests. Its ability at wall scale was also confirmed by reproducing the pushover experimental program reported in Mehrabi and Shing [20]. The corresponding simulations are presented in [67,68]. During the current experiments, it was not possible to reach the peak of strength of the four CM walls, because of the excessive solicitation and the risk of instabilities. Consequently, the numerical model was used to predict the complete load-displacement curve of the tested samples. The aim is to study the maximum strength and the post-peak response of the two types adopted (uniform and toothed confinement). The previously described model was used (section 4.1) while keeping the same materials parameters (table 8). Boundary conditions (Fig. 13) are also the same, except to a more important horizontal displacement in order to overtake the maximal strength capacity of the walls. The obtained loading-displacement curves for all cases are shown in figure (18).

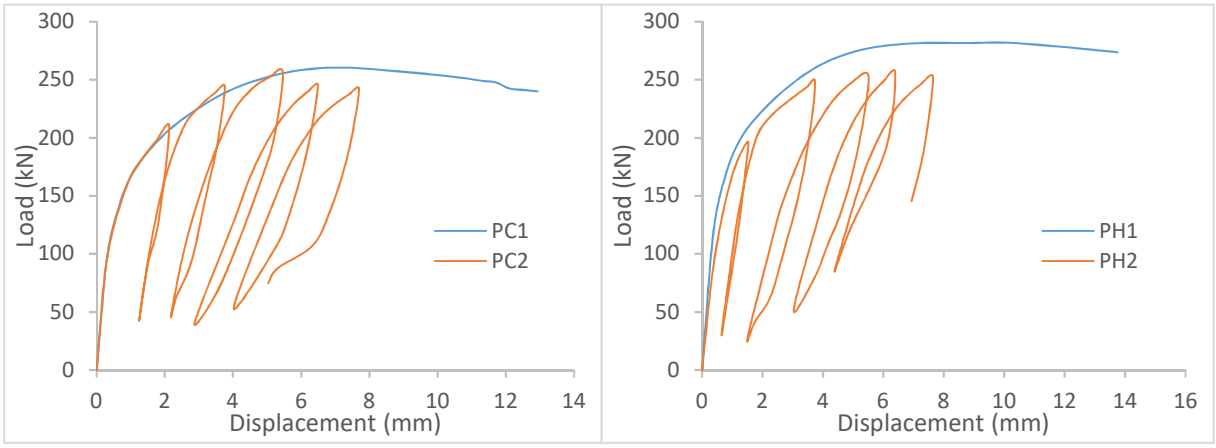

Fig. 18: *Complete numerical load-displacement curves of samples PC1, PC2, PH1 and PH2.*

The numerical extended curves allow us to deduce the maximal lateral resistance of each sample, and consequently compare the two construction types in term of strength. The sample with uniform confinements reached a strength of 260.5 kN under monotonic lateral loading (PC1) and 257.2 kN under the loading-unloading condition (PC2) while the CM walls with toothed connections reached a strength of 282.1 kN in the case of the monotonic condition (PH1) and 256.5 kN in the case of the loading-unloading condition (PH2). It should be noted that these values are close to those assessed experimentally from the curves (see Table 2). This confirms that the lateral strength was almost reached during the experimental phase. Comparing the sample types, the toothed sample resists a little more than the uniform one. In the case of monotonic tests, the use of toothed masonry confinements improves the lateral resistance by 8.29%, but no improvement was recorded in the case of cyclic tests. The obtained ratio demonstrates that the toothing of the confinement elements in CM walls has not increased the strength significantly. Similar results have been found in the work of Matošević et al. and also Wijaya et al. [56,69].

6. Conclusion

This paper reports an analytical and a numerical study on the behavior of confined masonry walls in monotonic as well as loading-unloading conditions. Based on the obtained results and the observations during the tests, the following conclusions can be drawn:

1. Regarding the assessed analytical models in this study, the model of Rai et al. [49] and Riahi et al. [50] respectively underestimated and overestimated significantly the stiffness of all the samples. The model of Flores and Alcocer [21] satisfactorily predicted the initial rigidity of the walls, in which the ratio values obtained stand within the interval ($0.96 \leq K_{cal} / K_{exp} \leq 1.10$) for all the samples. In the case of the first crack strength, the model of Matsumura, Standard Chilean and Moroni et al. [26,51,52] underestimated the first crack strength as long as the obtained ratios are significantly low ($V_{cal} / V_{exp} \leq 0.82$). The model proposed by Flores and Alcocer [21] overestimated the first crack strength ($1.12 \leq V_{cal} / V_{exp} \leq 1.6$) but still stands as a good approximation indicator. The best results have been found using the model of Riahi et al [50], where various obtained ratios remained within the interval [0.99; 1.41]. Regarding the peak strength prediction, Marques and Lourenço [53] model's overestimated the peak strength ($1.43 \leq V_{cal} / V_{exp} \leq 1.55$), also the model of Rai et al. [24] overestimated this strength but still stands as a good indicator where the ratio values obtained stand within interval [1.1 ; 1.9]. The model of Riahi et al. [25] underestimated the peak strength in all the cases (for all samples). The best predicting model, in a conservation way, corresponds to the model of Castilla and Marinilli [54] ($0.88 \leq V_{cal} / V_{exp} \leq 0.95$).

2. A finite elements model was adopted and introduced in Cast3m software, which offered an optimal choice as far as calculation cost and precision are concerned. It was also able to simulate the global response, cracking paths and failure modes of all partial structures including an interface element under three-point bending tests, masonry triplet under shear tests, masonry panel under vertical compression test and masonry panel under diagonal compression test. Furthermore, the model has properly simulated the behavior of CM walls (with uniform and toothed confinements) under lateral loading when combined with vertical load. It was able to significantly reproduce the response of all samples in terms of loading-displacement curves, failure modes, cracks propagation paths, rigidity degradation and energy dissipation capacities.

3. Curves responses of the tested samples were extended using the validated model. Therefore, the CM walls with toothed confining elements as well as uniform confining elements' lateral strengths were compared. Based on this comparison, the results of Wijaya et al.[69] and Matošević et al.[70] has been confirmed, the toothing of confining elements does not improve the lateral strength of the CM walls.

The numerical model used in the present paper was validated using some new and original experimental results. It will be used in the near future in the existing literature in order to generalize their techniques and their characterization process. Thanks to the simplified techniques adopted in the model, it can be used to analysis the behavior of small multi story buildings using powerful calculation machines. However, one of the drawbacks of the confined masonry walls is being highly rigid in the vertical direction, as the RC frame is cast in the masonry panel directly. It means that a significant ratio of the vertical loading is transmitted from the beam to the lower masonry panel, instead of being transmitted to the columns. Experience has shown that a building with more than one story may experience severe damage in case of seismic loading, when confined masonry panels are used. Hence, the main objective is to understand the real behavior the CM walls and consequently provides suitable macro models able to study the full scale buildings. Furthermore, the model will be used to study the seismic behavior and to deduce the Pushover curves of two story structures with uniform and toothed confined masonry double-panel walls.

Acknowledgements

This research was supported by Laboratoire Optimisation de la Conception et Ingénierie de l'Environnement (LOCIE) of the University of Savoie Mont Blanc - Le centre national de la recherche scientifique (CNRS), France

in partnership with the Laboratoire de génie civil appliqué (LGCA) of the University of Tebessa - La direction générale de la recherche scientifique et du développement technologique (DGRSDT), Algeria. Funding sources are gratefully acknowledged. Thanks are extended to: Pr. VACHER Pierre and Pr. Alain Sellier for providing the calculation software's and to Mr. Rabie Abderrahmane for providing language help.

References:

[1] D. Tripathy, V. Singhal, Estimation of in-plane shear capacity of confined masonry walls with and without openings using strut-and-tie analysis, Eng. Struct. 188 (2019) 290–304. https://doi.org/10.1016/j.engstruct.2019.03.002.

[2] A.I.O. Cruz, J.J.E. Pérez-gavilán, L.C. Flores, Experimental study of in-plane shear strength of con fi ned concrete masonry walls with joint reinforcement, Eng. Struct. 182 (2019) 213–226. https://doi.org/10.1016/j.engstruct.2018.12.040.

[3] A. Chourasia, S. Singhal, J. Parashar, Experimental investigation of seismic strengthening technique for confined masonry buildings, J. Build. Eng. 25 (2019) 100834. https://doi.org/https://doi.org/10.1016/j.jobe.2019.100834.

[4] H. M. Seif Eldin, N. Aly, K. Galal, In-plane shear strength equation for fully grouted reinforced masonry shear walls, Eng. Struct. 190 (2019) 319–332. https://doi.org/10.1016/j.engstruct.2019.03.079.

[5] H. Alwashali, D. Sen, K. Jin, M. Maeda, Experimental investigation of influences of several parameters on seismic capacity of masonry infilled reinforced concrete frame, Eng. Struct. 189 (2019) 11–24. https://doi.org/10.1016/j.engstruct.2019.03.020.

[6] A. Costigan, S. Pavía, O. Kinnane, An experimental evaluation of prediction models for the mechanical behavior of unreinforced, lime-mortar masonry under compression, J. Build. Eng. 4 (2015) 283–294. https://doi.org/10.1016/j.jobe.2015.10.001.

[7] G. Henrique Nalon, C.F.R. Santos, L.G. Pedroti, J.C.L. Ribeiro, G. de S. Veríssimo, F.A. Ferreira, Strength and failure mechanisms of masonry prisms under compression, flexure and shear: Components' mechanical properties as design constraints, J. Build. Eng. 28 (2020) 101038. https://doi.org/https://doi.org/10.1016/j.jobe.2019.101038.

[8] A.E. Fiorato, M. a Sozen, W.L. Gamble, An Investigation of the Interaction of Reinforced Concrete Frames with Masonry Filler Walls, 1970.

[9] S. V Polyakov, On the Interaction between Masonry Filler Walls and Enclosing Frame when Loaded in the Plane of the Wall, Earthq. Eng. (1960) 36–42.

[10] M. Holmes, Steel Frames With Brickwork and Concrete Infilling, Proc. Inst. Civ. Eng. 19 (1961) 473–478. https://doi.org/https://doi.org/10.1680/iicep.1961.11305.

[11] B. Stafford Smith, Behaviour of Square Infilled Frames, Proc. Am. Soc. Civ. Eng. J. Struct. Div. (1966) 381–403.

[12] R.D. Flanagan, M.A. Tenbus, R.M. Bennett, Numerical modeling of clay tile infills, NCEER Work. Seism. Response Mason. Infills, San Fr. Calif. (1994) 63–68.

[13] F.J. Crisafulli, A.J. Carr, Proposed macro-model for the analysis of infilled frame structures, Bull. New Zeal. Soc. Earthq. Eng. 40 (2007) 69–77.

[14] R.E. Klingner, V. V Bertero, Earthquake Resistance of Infilled Frames, J. Struct. Div. 104 (1978) 973–989.

[15] I.N. Doudoumis, Finite element modelling and investigation of the behaviour of elastic infilled frames under monotonic loading, Eng. Struct. 29 (2007) 1004–1024. https://doi.org/10.1016/j.engstruct.2006.07.011.

[16] C.Z. Chrysostomou, Effects of degrading infill walls on the nonlinear seismic response of two-dimensional steel frames, Cornell university, 1991. https://doi.org/10.1021/pr900023z.

[17] T.C. Liauw, K.H. Kwan, Nonlinear Behavior Of Non-Integral Infilled Frames, Comput. Struct. Vol. 18 (1984) 551–560.

[18] T. Schmidt, An approach of modelling masonry infilled frames by the f.e. method and a modified equivalent strut model, Annu. J. Concr. Concr. Struct. 4 (1989) 171–180.

[19] R.H. Wood, Plasticity, composite action and collapse design of unreinforced shear wall panels in frames, Proc. Inst. Civ. Eng. 65 (1978) 381–411. https://doi.org/https://doi.org/10.1680/iicep.1978.2952.

[20] A.B. Mehrabi, P.B. Shing, Performance Of Masonry-Infilled Ric Frames Under In Plane Lateral Loads, Report no. CU/SR-94-6. Dept. of Civil, Environmental, and Architectural Engineering, University of Colorado, Boulder., 1994.

[21] L.E. Flores, S.M. Alcocer, Calculated response of confined masonry structures., Elev. World Conf. Earthq. Eng. (1996) Paper No. 1830.

[22] M. Tomaževič, I. Klemenc, Seismic behaviour of confined masonry walls, Earthq. Eng. Struct. Dyn. 26 (1997) 1059–1071. https://doi.org/10.1002/(SICI)1096-9845(199710)26:10<1059::AID-EQE694>3.0.CO;2-M.

[23] A. Bourzam, T. Goto, M. Miyajima, Shear Capacity Prediction of Confined Masonry Walls Subjected To Cyclic Lateral Loading, Doboku Gakkai Ronbunshuu A. 64 (2008) 692–704. https://doi.org/10.2208/jsceseee.25.47s.

[24] D.C. Rai, V. Singhal, S. Paikara, D. Mukherjee, Sub-paneling of masonry walls using precast reinforced concrete elements for earthquake resistance, Earthq. Spectra. 30 (2014) 913–937. https://doi.org/10.1193/102010EQS178M.

[25] Z. Riahi, K.J. Elwood, S.M. Alcocer, Backbone Model for Confined Masonry Walls for Performance-Based Seismic Design, J. Struct. Eng. 135 (2009) 644–654. https://doi.org/10.1061/(ASCE)ST.1943-541X.0000012.

[26] M.O. Moroni, M. Astroza, S. Tavonatti, Nonlinear models for shear failure in confined masonry walls, Mason. Soc. J., 12_2_, 72–78. (1994).

[27] E. D'Amore, L. Decanini, Shear strength analysis of confined masonry panels under cyclic loads: comparison between proposed expressions and experimental data, 9th Int. Semin. Earthq. Progn. (1994).

[28] A. Marinilli, E. Castilla, Experimental Evaluation of Confined Masonry Walls with Several Confining-Columns, 13th World Conf. Earthq. Eng. 2129 (2004).

[29] A. San Bartolomé, D. Quiun, P. Myorca, Proposal of a standard for seismic design of confined masonry buildings, Bull. ERS,. 37 (2004).

[30] A. Matsumura, Shear strength of reinforced masonry walls, 9th World Conf. Earthq. Eng. Vol. 6 (1988) 121–126.

[31] M. Tomaževič, I. Klemenc, Verification of seismic resistance of confined masonry buildings, Earthq. Eng. Struct. Dyn. 26 (1997) 1073–1088.

[32] M. Lafuente, E. Castilla, C. Genatios, Experimental and analytical evaluation of the seismic resistant behaviour of masonry walls., Mason. Int. 11 (1998) 80–88.

[33] N. Bicanic, C. Stirling, C.J. Pearce, Discontinuous Modelling of Structural Masonry, Fifth World Congr. Comput. Mech. Vienna, Austria. (2002) 18 pages.

[34] F.J. Crisafulli, Seismic Behaviour of Reinforced Concete Structures with Masonry Infills, university of Canterbury Christchurch, New Zealand, 1997.

[35] D. Combescure, Modélisation du comportement sous chargement sismique des structures de bâtiment comportant des murs de remplissage en maçonnerie, Ecole Centrale Paris, France, 1996.

[36] A. Page, Finite element model for masonry, Proc. a Sess. Held Conjunction with Struct. Congr. (1978).

[37] J.I. Cruz Diaz, Etude des murs de contreventement en maçonnerie d'éléments de terre cuite, Université de Marne-la-Vallée, 2002.

[38] P.B. Lourenço, L.F. Ramos, Characterization of Cyclic Behavior of Dry Masonry Joints, J. Struct. Eng. 130 (2004) 779–786.

[39] D. Oliveira, P. Lourenço, E. Garbin, Experimental investigation on the structural behaviour and strengthening of three-leaf stone masonry walls, Struct. Anal. Hist. Constr. (2006) 817–826.

[40] A.B. Mehrabi, P.B. Shing, Seismic Analysis of Masonry-Infilled Reinforced Concrete Frames, TMS J. (2003) 81–94.

[41] G. Al-chaar, A.B. Mehrabi, T. Manzouri, Finite Element Interface Modeling and Experimental Verification of Masonry-infilled R / C Frames, TMS J. (2008) 9–27.

[42] G. Baloević, J. Radnić, A. Harapin, Numerical dynamic tests of masonry-infilled RC frames, Eng. Struct. 50 (2013) 43–55. https://doi.org/10.1016/j.engstruct.2012.11.034.

[43] A. Rahman, S.C. Anand, Empirical Mohr-Coulomb failure criterion for concrete block-mortar joints, J. Struct. Eng. 120 (1995) 2408–2422.

[44] P.B. Lourenço, Computational strategies for masonry structures, université de technologie de Delft, 1996. https://doi.org/ISBN 90-407-1221-2.

[45] D. j. Sutcliffe, H.S. Yu, A.W. Page, Limit analysis of anisotropic or jointed media-application to unreinforced masonry shear walls, 12 Th Int. BRICK/BLOCK Mason. Conf. (2001) 1765–1776.

[46] J.I. Cruz-diaz, A. Sellier, B. Capra, P. Delmotte, P. Rivillon, A. Mebarki, Modélisation simplifiée du comportement à rupture des murs, Rev. Française Génie Civ. 5 (2001) 613–627. https://doi.org/10.1080/12795119.2001.9692714.

[47] L. Abdou, R. Ami Saada, F. Meftah, A. Mebarki, Mechanical study of the behavior of masonry walls: Numerical results and sensitivity analysis, Constr. Build. Des. Mater. Tech. (2011) 211–233.

[48] C. Belghiat, A. Messabhia, J.-P. Plassiard, M. Guenfoud, O. Plé, P. Perrotin, Experimental study of double-panel confined masonry walls under lateral loading, J. Build. Eng. 20 (2018). https://doi.org/10.1016/j.jobe.2018.09.001.

[49] D.C. Rai, V. Singhal, S. Paikara, D. Mukherjee, Sub-paneling of masonry walls using precast reinforced concrete elements for earthquake resistance, Earthq. Spectra. 30 (2014) 913–937. https://doi.org/10.1193/102010EQS178M.

[50] Z. Riahi, K.J. Elwood, S.M. Alcocer, Backbone Model for Confined Masonry Walls for Performance-Based Seismic Design, J. Struct. Eng. 135 (2009) 644–654. https://doi.org/10.1061/(ASCE)ST.1943-541X.0000012.

[51] INN-1997., Albanileria confinada-requisitos de deseno y calculo., Instituto Nacional de Normalizacion, Santiago, Chile, 1997.

[52] A. Matsumura, Shear strength of reinforced masonry walls, 9th Worrld Conf. Earthq. Eng. Vol. 6 (1988) 121–126.

[53] R. Marques, P.B. Lourenço, A model for pushover analysis of confined masonry structures: Implementation and validation, Bull. Earthq. Eng. (2013). https://doi.org/10.1007/s10518-013-9497-5.

[54] E. Castilla, A. Marinilli, Seismic Behavior of Confined Masonry Walls with Intermediate Confining-Columns, 8th U.S. Natl. Conf. Earthq. Eng. (2006).

[55] V. Singhal, D.C. Rai, In-plane and out-of-plane behavior of confined masonry walls for various toothing and openings details and prediction of their strength and stiffness, Earthq. Eng. Struct. Dyn. 45 (2016) 2551–2569. https://doi.org/10.1002/eqe.2783.

[56] Đurđica Matošević, V. Sigmund, I. Guljaš, Cyclic testing of single bay confined masonry walls with various connection details, Bull. Earthq. Eng. 13 (2014) 565–586. https://doi.org/10.1007/s10518-014-

9627-8.

[57] A. Sellier, G. Casaux-Ginestet, L. Buffo-Lacarrière, X. Bourbon, Orthotropic damage coupled with localized crack reclosure processing, Part 1: Constitutive laws, Eng. Fract. Mech. 97 (2013) 148–167.

[58] A. Sellier, Anisotropic Damage and Visco-Elasto-Plasticity Applied to Multiphasic Materials, LMDC - Lab. Matériaux Durabilité Des Constr. Toulouse ; Univ. Toulouse III - Paul Sabatier; Insa Toulouse. (2018).

[59] P. Pegon, A. V. Pinto, M. Géradin, Numerical modelling of stone-block monumental structures, Comput. Struct. 79 (2001) 2165–2181. https://doi.org/10.1016/S0045-7949(01)00070-0.

[60] P.G. Asteris, V. Plevris, V. Sarhosis, L. Papaloizou, A. Mohebkhah, P. Komodromos, Numerical modeling of historic masonry structures, 2015. https://doi.org/10.4018/978-1-4666-8286-3.ch007.

[61] N. Domede, A. Sellier, T. Stablon, Structural analysis of a multi-span railway masonry bridge combining in situ observations, laboratory tests and damage modeling, Eng. Struct. 56 (2013) 837–849.

[62] A. Drougkas, P. Roca, C. Molins, Numerical prediction of the behavior, strength and elasticity of masonry in compression, Eng. Struct. 90 (2015) 15–28. https://doi.org/10.1016/j.engstruct.2015.02.011.

[63] P. Vacher, S. Dumoulin, F. Morestin, S. Mguil-Touchal, Bidimensional strain measurement using digital images, Proc. Inst. Mech. Eng. Part C J. Mech. Eng. Sci. 213 (1999) 811–817. https://doi.org/10.1243/0954406991522428.

[64] ASTM E 519-02, Standard Test Method for Diagonal Tension (Shear) in Masonry Assemblages, Am. Soc. Test. Mater. (2002) 5. https://doi.org/10.1520/E0519.

[65] P. Vacher, S. Dumoulin, F. Morestin, S. Mguil-Touchal, Bidimensional strain measurement using digital images, Proc. Inst. Mech. Eng. Part C J. Mech. Eng. 213 (1999) 811–817. https://doi.org/10.1243/0954406991522428.

[66] R. SHAAN, J.-M. TORRENTI, Etude expérimentale de la maçonnerie sous sollicitations uniaxiales et biaxiales, Inst. Tech. Batim. Des Trav. Publics. Essais et (1990). https://doi.org/ISSN 0020-2568.

[67] C. Belghiat, Contribution à la modélisation dynamique de la maçonnerie chaînée, Ph-D thesis, soutenance du 19 septembre 2019. Université du Larbi Tébessi - Université Savoie Mont Blanc, 2019.

[68] C. Belghiat, J. Plassiard, P. Perrotin, O. Plé, M. Guenfoud, A. Messabhia, Contribution à la modélisation dynamique de la maçonnerie chainée, Acad. J. Civ. Eng. 1 (2016) 32–40. https://doi.org/doi:10.26168/ajce.34.1.32.

[69] W. Wijaya, D. Kusumastuti, M. Suarjana, Rildova, K. Pribadi, Experimental study on wall-frame connection of confined masonry wall, Procedia Eng. 14 (2011) 2094–2102. https://doi.org/10.1016/j.proeng.2011.07.263.

[70] Đ. Matošević, V. Sigmund, I. Guljaš, Cyclic testing of single bay confined masonry walls with various connection details, Bull. Earthq. Eng. 13 (2014) 565–586. https://doi.org/10.1007/s10518-014-9627-8.